Proceedings of Australasian Conference on Robotics and Automation, 3-5 Dec 2012, Victoria University of Wellington, New Zealand.

# Motion Planning of a Planar 3R Manipulator Utilising Fluid Flow Trajectory Generation

**Darwin Lau, Jonathan Eden and Denny Oetomo**
The University of Melbourne, Australia
laudt@unimelb.edu.au, j.eden2@student.unimelb.edu.au and doetomo@unimelb.edu.au

## Abstract

A novel approach to perform motion planning on 2 or 3 degrees-of-freedom manipulators utilising a fluid motion planning model is proposed. It is demonstrated that through the introduction of transformations, the conventional trajectory planning problem in the configuration space (*C-space*) can be efficiently solved from the closed form solution of the fluid motion planner. The proposed motion planner is designed to be computationally efficient for real-time implementation and dynamic environments. The manipulator fluid motion planner is demonstrated on a 3-DoF 3-revolute ($3R$) planar manipulator example. The results show the simplicity, effectiveness and potential of the proposed novel method in manipulator motion planning.

## 1 Introduction

The motion planning problem for robotic systems can be described as the generation of a trajectory between an initial and a final configuration, under a set of constraints. Constraints can include the avoidance of obstacles, and limitations in speed and acceleration. In the motion planning of mobile robots, the problem is simplified by assuming the system to be a point particle. As such, obstacle avoidance only requires the resulting trajectory to not collide with any obstacles. In comparison, motion planning for rigid body manipulators is more complicated as the entire rigid body must avoid collision with the environment.

A common approach for manipulator motion planning is to the perform the trajectory generation in the configuration space (*C-space*) of the system [Maciejewski and Fox, 1993; Kavraki *et al.*, 1996; Lin *et al.*, 2005; Kuffner and LaValle, 2000]. The C-space is expressed with respect to the generalised coordinates of the manipulator where obstacles represents the poses in which any part of the manipulator collides with the environment. Consequently, the *free space* within the C-space represents the poses in which the manipulator does not collide with the environment. The manipulator motion planning problem can be divided into two stages, the construction of the C-space and the generation of a continuous trajectory within the free space.

Various approaches have been studied in manipulator motion planning. Sampling techniques [Kavraki *et al.*, 1996; Kuffner and LaValle, 2000; Karaman and Frazzoli, 2011] are numerical search approaches that takes probabilistic samples to construct and navigate within the C-space. Geometric [Kircanski and Timcenko, 1992; Chirikjian and Burdick, 1992; Yahya and Mohamed, 2009], neural network [Mao and Hsia, 1997; Zhang *et al.*, 2009; Yang and Meng, 2000] and Artificial Potential Field ($APF$) [Lin *et al.*, 2005; Khatib, 1986; Fahimi *et al.*, 2003] based approaches construct the free space geometrically and determines the trajectory either by a set of splines of a known form, neural networks or potential functions, respectively.

In the motion planning of mobile robots, fluid-based motion planners have been studied as an efficient approach to analytically determine the velocity of the desired trajectory [Li and Bui, 1998; Waydo and Murray, 2003]. Fluid motion planners are a class of APF techniques, where established differential equations in fluid mechanics form harmonic potential function. The main limitations of this approach are that it can only operate within 2-D and 3-D environments and avoids only a limited range of obstacles, such as spheres and planes.

In this paper, a novel fluid flow model based motion planning algorithm for rigid link manipulators with two and three degrees-of-freedom ($DoF$) is proposed. A transformed C-space, termed as *S-space*, is introduced to increase the range of obstacles that can be avoided. Motion planning is performed within the S-space utilising the fluid flow motion planner. From the expressions of the trajectory velocity from the fluid flow model, it is shown that the derivative of the generalised coordinate

for the desired manipulator motion can be analytically expressed. The S-space transformations and proposed manipulator fluid motion planning algorithm is demonstrated on a 3-DoF 3-revolute (*3R*) planar manipulator example.

The remainder of the paper is organised as follows: Section 2 presents the fundamental concepts of fluid motion planning studied in mobile robots. Section 3 defines the proposed S-space and demonstrates the mapping on a 3R planar manipulator. The framework for the manipulator fluid motion planning algorithm is presented in Section 4. The motion planning for a 3R planar manipulator is simulated and the results are shown in Section 5. Finally, Section 6 concludes the paper and presents areas of future work.

## 2 Background on Fluid Motion Planning

In this section, the governing equations for fluid motion planning of 2-D and 3-D mobile robots are described. The fluid flow model for the motion planner is shown in Figure 1, where the robot is located at position $\mathbf{s}$ and the target destination is modelled as a sink (attraction) element located at position $\mathbf{s_d}$. For non-holonomic systems, to ensure that the heading direction $\mathbf{d}$ is satisfied, a source (repulsion) element is located directly behind the robot at position

$$\mathbf{s_s} = \mathbf{s} - \Delta d \cdot \mathbf{d} \ , \tag{1}$$

where $\Delta d > 0$ represents a constant distance between the robot and the source location behind the robot position.

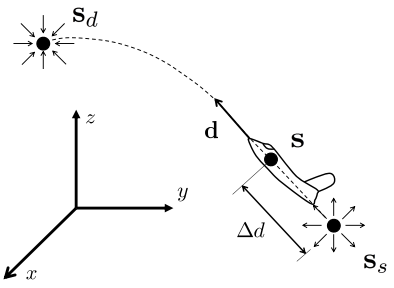


Figure 1: Fluid flow motion planner model

The 2-D and 3-D potential functions, $\phi_{2d}$ and $\phi_{3d}$, respectively, for the described model can be expressed as

$$\begin{aligned} \phi_{2d} &= \frac{Q_s}{2\pi}\log\left(||\mathbf{s}-\mathbf{s_s}||\right) - \frac{Q_d}{2\pi}\log\left(||\mathbf{s}-\mathbf{s_d}||\right), \\ \phi_{3d} &= -\frac{Q_s}{4\pi\,||\mathbf{s}-\mathbf{s_s}||} + \frac{Q_d}{4\pi\,||\mathbf{s}-\mathbf{s_d}||}, \end{aligned} \tag{2}$$

where $Q_s > 0$ and $Q_d > 0$ represents the strengths of the source and sink elements, respectively. The velocity vector $\dot{\mathbf{s}}$ for the desired trajectory can be determined by taking the gradient of the potential functions from (2). Hence, explicit expressions for the velocity vector in 2-D and 3-D can be determined by solving $\dot{\mathbf{s}} = \nabla\phi_{2d}$ and $\dot{\mathbf{s}} = \nabla\phi_{3d}$, respectively.

### 2.1 Sphere Avoidance

The 2-D and 3-D sphere theorems [Weiss, 1944] can be utilised to produce the potential functions $\phi_{s2d}$ and $\phi_{s3d}$ for the flow around a circle and a sphere, respectively. The transform can be expressed with respect to the potential functions from (2) as

$$\begin{aligned} \phi_{s2d} &= \phi_{2d}(\mathbf{s}) + \phi_{2d}\left(\frac{R^2\mathbf{s}}{||\mathbf{s}||^2}\right) \ , \\ \phi_{s3d} &= \phi_{3d}(\mathbf{s}) + \frac{R}{||\mathbf{s}||}\phi_{3d}\left(\frac{R^2\mathbf{s}}{||\mathbf{s}||^2}\right) \\ &\quad -\frac{2}{R\,||\mathbf{s}||}\int_0^R x\phi_{3d}\left(\frac{x^2\mathbf{s}}{||\mathbf{s}||^2}\right)dx \ , \end{aligned} \tag{3}$$

where $R$ represents the radius of the circle or sphere. The velocity vector $\dot{\mathbf{s}}$ for the 2-D and 3-D trajectories can be determined by solving $\dot{\mathbf{s}} = \nabla\phi_{s2d}$ and $\dot{\mathbf{s}} = \nabla\phi_{s3d}$, respectively.

Hence from (3), analytical expressions for the components of the resulting trajectory velocity can be determined. The final motion trajectory $\mathbf{s}(t)$ can then be determined by performing numerical integration on $\dot{\mathbf{s}}$. The advantage of this motion planning approach is that it is computationally efficient in generating a natural trajectory to avoid spherical obstacles.

### 2.2 Multiple Obstacle Avoidance

Multiple obstacle avoidance for fluid flow motion planners have been proposed in [Waydo and Murray, 2003]. In this method, the final trajectory is determined by applying a weighted superposition on the trajectories for each individual obstacle. The weights depend on the distance between the robot and each of the obstacles. The velocity of the trajectory in an $n$ obstacle environment can be expressed as

$$\dot{\mathbf{s}} = \sum_{i=1}^{n} \alpha_i \dot{\mathbf{s}}_i \ , \tag{4}$$

where $\alpha_i$ and $\dot{\mathbf{s}}_i$ represents the weight and trajectory velocity for a single obstacle $i$, respectively. In the proposed path planner, the weighting $\alpha_i$ is defined as

$$\alpha_i = \prod_{j\neq i}^{n} \frac{d_j^4}{d_i^4 + d_j^4} \ , \tag{5}$$

where $d_i$ represents the distance between the robot and obstacle $i$. The final trajectory for multiple obstacle avoidance can be determined by numerically integrating $\dot{\mathbf{s}}$ from (4).

## 3 Fluid C-space for 3R Manipulators

The C-space in manipulator motion planning represents the environment expressed with respect to the generalised coordinates of the manipulator. Obstacles in C-space represent the poses in which any part of the manipulator will collide with the environment. For an $n$-DoF manipulator, the generalised coordinates and the C-space are $n$-dimensional and can be denoted by $\mathbf{q}$ and $\mathbb{Q}^n$, respectively, where $\mathbf{q} \in \mathbb{Q}^n$.

Despite the computational efficiency and simplicity of the fluid motion planning algorithm described in Section 2, the method is limited to the avoidance of spherical obstacles. To relax this limitation, a transformation is introduced between the C-space and the space in which fluid motion planning (*S-space*) is performed. Denoting an $n$-dimensional S-space as $\mathbb{S}^n$, the transformation $f : \mathbb{S}^n \Rightarrow \mathbb{Q}^n$ can be represented by the function

$$\mathbf{q} = f(\mathbf{s}) \ . \tag{6}$$

To ensure that the resulting trajectories in $\mathbb{Q}^n$ are continuous and well formed, it is necessary that the mapping $f$ is a continuous and one-to-one function.

To illustrate the mapping and representation of obstacles for the manipulator C-space, considering the 3-DoF 3-revolute ($3R$) planar manipulator shown in Figure 2. The generalised coordinates for the system can be represented by $\mathbf{q} = [q_1 \ q_2 \ q_3]^T$, where $q_1$, $q_2$ and $q_3$ are the absolute angles for links 1, 2 and 3, respectively. From the lengths of links 1, 2 and 3, denoted by $l_1$, $l_2$ and $l_3$, respectively, and the generalised coordinates $\mathbf{q}$, the position of the end effector $\mathbf{x}_e$ can be determined. In the examples in this paper, the lengths of the manipulator links were set to $l_1 = l_2 = l_3 = 1$.

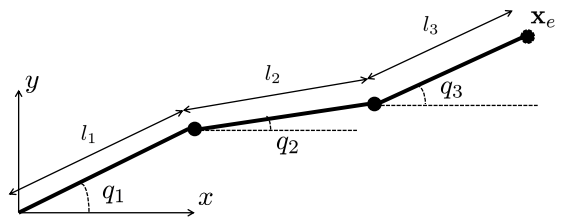




Figure 2: 3-DoF 3R planar manipulator model

### 3.1 S-space Obstacles in C-space

Consider the trivial mapping $\mathbf{q} = \mathbf{s}$, which results in a sphere obstacle of radius $R$ in $\mathbb{Q}^3$. Figure 3 shows the manipulator configurations for a set of randomly selected poses that lie on the surface of a sphere of radius $R = 1$. The dashed line corresponds to the approximate boundary between the valid and invalid end effector positions.

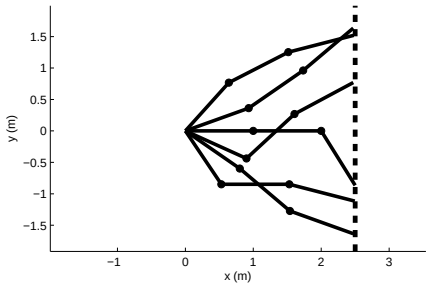


Figure 3: Example manipulator configurations for poses on the surface of a sphere where $R = 1$

From the configurations, it can be observed that the boundary poses for a sphere obstacle in $\mathbb{Q}^3$ corresponds to approximately a vertical wall boundary. To illustrate the effect of the sphere obstacle, two configurations, one representing a pose inside and the other outside the sphere, are shown in Figures 4. Figure 4(a) shows the configuration of a pose outside of the sphere ($||\mathbf{q}|| > R$). Lying outside the S-space obstacle, this configuration can be considered as valid since the manipulator is not in collision with the wall, represented by the dashed lines. Figure 4(b) shows the configuration of a pose within the invalid region of the S-space ($||\mathbf{q}|| < R$). This configuration is an invalid one as the manipulator collides with the wall boundary.

From the example configurations, it can be observed that a trajectory in C-space avoiding the spherical obstacle corresponds to motion for the 3R manipulator avoiding collision with the wall boundary. Hence, a valid trajectory for the 3R manipulator can be generated by performing motion planning within the S-space.

To illustrate the potential of transformations, the following mapping transforms a sphere in $\mathbb{S}^3$ to a cube with rounding edges and vertices in $\mathbb{Q}^3$

$$q_1 = \sqrt[3]{s_1}, q_2 = \sqrt[3]{s_2}, q_3 = \sqrt[3]{s_3} \ , \tag{7}$$

where $\mathbf{q} = [q_1 \ q_2 \ q_3]^T$ and $\mathbf{s} = [s_1 \ s_2 \ s_3]^T$. Figure 5(a) shows the resulting transformed obstacle in $\mathbb{Q}^3$. Figure 5(b) shows the configurations for a sample of poses on the obstacle surface, where the dashed line represents the resulting boundary.

### 3.2 Transforms for C-space Obstacles

Section 3.1 introduced the concept of how mappings of S-space can result in different obstacles in C-space. In this section, the method to create mappings to S-space

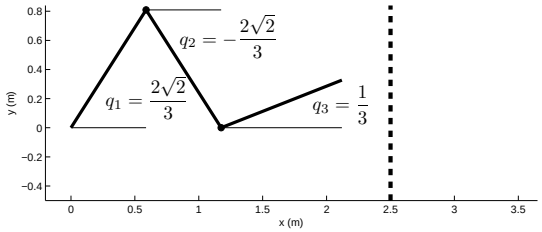


(a) Valid configuration where $||\mathbf{q}|| = 1.4$

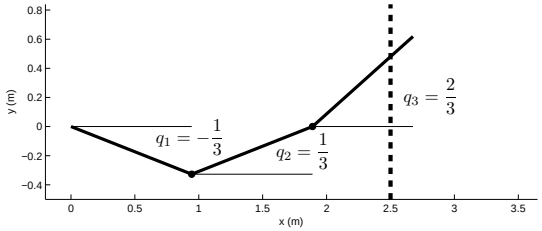


(b) Invalid configuration where $||\mathbf{q}|| = 0.8$

Figure 4: Example manipulator configurations for poses outside and inside the sphere obstacle

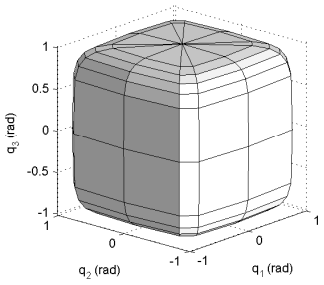


(a) Obstacle in $\mathbb{Q}^3$

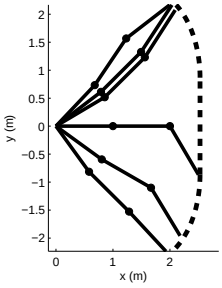


(b) Configurations for poses on obstacle surface

Figure 5: Rounded edge and vertex cube obstacle

from obstacles in C-space will be described. To illustrate the procedure, the C-space and S-space environments to result in a wall obstacle for a 3R manipulator will be determined.

From Section 3.1, it was shown that a sphere obstacle in C-space results in a vertical wall boundary for a 3R manipulator where the lengths of all the links are equal. The shape of the obstacle was determined by observing the invalid end effector $\mathbf{x}_e$ positions, resulting in the set of poses in which the third link will collide with the wall. Similarly, it can be observed that the avoidance of a wall for link 3 of a 3R manipulator with non-equal link lengths $l_1$, $l_2$ and $l_3$ result in an ellipsoid in C-space. Denoting the $x$ position of the wall as $k$, the radii of the ellipsoid in dimensions $q_1$, $q_2$ and $q_3$, denoted by $r_1$, $r_2$ and $r_3$, respectively, can be expressed as

$$\begin{aligned} r_1 &= \cos^{-1}\frac{k - l_2 - l_3}{l_1}, \\ r_2 &= \cos^{-1}\frac{k - l_1 - l_3}{l_2}, \\ r_3 &= \cos^{-1}\frac{k - l_1 - l_2}{l_3}. \end{aligned} \tag{8}$$

The corresponding mapping from S-space with a sphere radius $R$ can be expressed as

$$q_1 = \frac{r_1}{R}s_1, q_2 = \frac{r_2}{R}s_2, q_3 = \frac{r_3}{R}s_3\ . \tag{9}$$

It should be noted that for wall distances $k \leq l_1 + l_2$, it is possible for link 2 to collide with the wall independent to the pose of link 3. In a similar manner to the collision of link 3, the resultant C-space obstacle is an elliptical column with its cross-section in the $q_1$ and $q_2$ plane. The column extends in the $q_3$ dimension as the collision between link 2 and the wall is independent to $q_3$. The $q_1$ and $q_2$ radii of the elliptical column, denoted by $r_1$ and $r_2$, respectively, can be expressed as

$$r_1 = \cos^{-1}\frac{k - l_2}{l_1}, r_2 = \cos^{-1}\frac{k - l_1}{l_2}\ . \tag{10}$$

Note that the avoidance of an elliptical column can be achieved by performing 2-D fluid motion planning about a circle in $q_1$ and $q_2$, and $q_3$ can be determined by linearly interpolating between the initial and final poses. Hence, wall avoidance for the 3R manipulator results from the superposition of the ellipsoid and elliptical column obstacles, as shown in Figure 6.

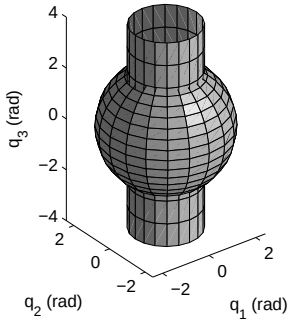


Figure 6: C-space representation of wall obstacle

In this case the end effector positions are sufficient in generating an obstacle mapping for all points of the rigid body due the nature of the wall obstacle. In general the C-space mapping would be performed such that the obstacle was mapped for all points of the rigid body. Once

the suitable C-space obstacle is determined a mapping from the S-space to the C-space in the form of (6) can be applied provided that the necessary mapping is one to one and continuous.

## 4 Manipulator Fluid Motion Planning Framework

Manipulator motion planning within the C-space can be efficiently determined utilising the fluid motion planning strategy described in Section 2 and the transformation between C-space and S-space introduced in Section 3. The motion planning problem can be described as reaching a final pose $\mathbf{q}_d$ from the current pose $\mathbf{q}$. To ensure that continuity in C-space is satisfied, a source element located at $\mathbf{q}_s$ can be determined by (1).

Deriving from (6), the velocity of the C-space trajectory can be analytically determined by

$$\dot{\mathbf{q}} = \dot{\mathbf{s}} f'(\mathbf{s}) \ . \tag{11}$$

The S-space trajectory velocity $\dot{\mathbf{s}}$ from (4), requires the manipulator pose $\mathbf{s}$, source element location $\mathbf{s}_s$ and sink element location $\mathbf{s}_d$ to be expressed in S-space. These can be determined by applying the inverse mapping $f^{-1}$ of (6) on $\mathbf{q}$, $\mathbf{q}_s$ and $\mathbf{q}_d$. Finally, the desired C-space trajectory $\mathbf{q}(t)$ can be determined by integrating $\dot{\mathbf{q}}$ from (11).

To illustrate the proposed C-space motion planning strategy that utilises fluid motion planning in S-space, consider the example scenario shown in Figure 7. The example scenario shows the avoidance of a cube obstacle with the mapping from (7). From the initial and final C-space poses shown in Figure 7(b), the S-space trajectory that results from the fluid motion planning method described in Section 2 is shown in Figure 7(a).

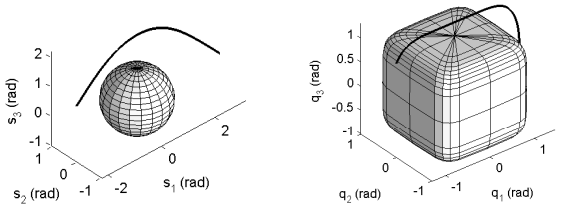


(a) S-space trajectory (b) Final C-space trajectory

Figure 7: Example of S-space and C-space trajectories

The corresponding trajectory in C-space is shown in Figure 7(b). The trajectory was determined by mapping the S-space derivative $\dot{\mathbf{s}}$ to the C-space derivative $\dot{\mathbf{q}}$ at each instant in time using (11). From the resulting trajectories, it can be observed that the naturally shaped motion around the sphere obstacle is preserved in the avoidance of a cube obstacle in C-space. Additionally, the continuity of the trajectory in the S-space is preserved in the C-space since the mapping function from (11) is continuous and one-to-one.

## 5 Simulation and Results

To demonstrate the proposed manipulator fluid motion planning strategy presented in Section 4, the motion planning for a 3R manipulator is shown in this section. The links of the 3R manipulator are of equal length, where $l_1 = l_2 = l_3 = 1$. Two vertical wall obstacles are situated at $x = 1.25$ and $x = -1.25$, on either side of the manipulator.

In the first scenario, the wall obstacles were not considered and the fluid motion planning strategy in the absence of any obstacles was utilised. Figure 8 shows a sequence of 4 frames at times $t = t_0, t_1, t_2, t_3$, where $t_0 < t_1 < t_2 < t_3$, for configurations from the initial pose (straight down) to the final pose (straight up).

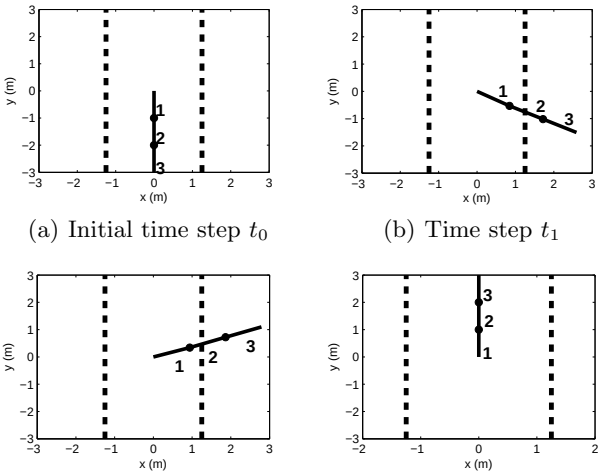


(a) Initial time step $t_0$ (b) Time step $t_1$

(c) Time step $t_2$ (d) Final time step $t_3$

Figure 8: Resulting configurations for trajectory not considering wall obstacles

Figures 8(b) and 8(c) show two intermediate snapshots of the manipulator's configuration in reaching the desired final pose. In this scenario, the fluid flow motion planner produces the expected natural trajectory where all three links are fully extended for the entire time of motion. The manipulator would collide with the wall at $x = 1.25$ if the wall obstacles, represented by the dashed lines, were present and hence would result in an invalid trajectory.

In the second scenario, the two wall obstacles were considered in the motion planner. For the same initial and final poses as the previous scenario, the resulting

motion is shown through a sequence of six frames at times $t_0 < t_1 < t_2 < t_3 < t_4 < t_5$ in Figure 9.

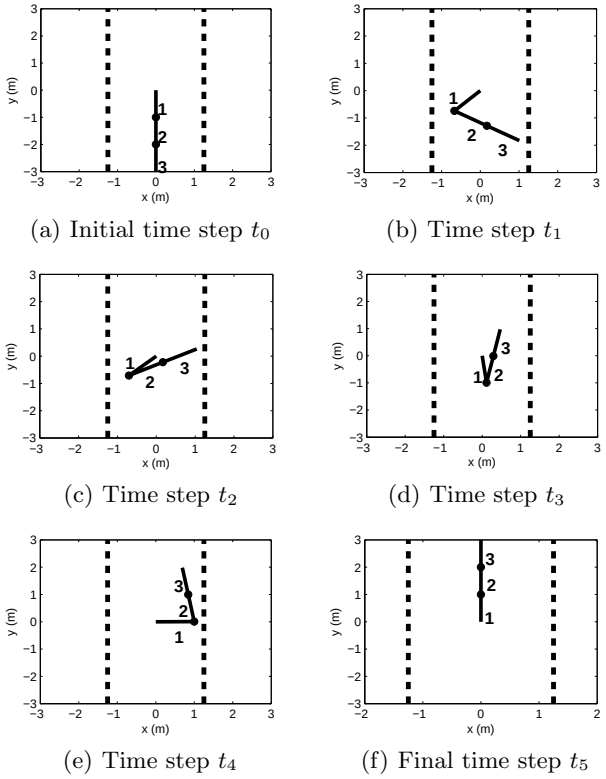


(a) Initial time step $t_0$ (b) Time step $t_1$

(c) Time step $t_2$ (d) Time step $t_3$

(e) Time step $t_4$ (f) Final time step $t_5$

Figure 9: Resulting configurations for trajectory considering wall obstacles

The resulting motion is significantly different to the motion if obstacles were not considered. To avoid the walls, the links of the manipulator would be required to fold inwards. At times $t_1$ and $t_2$, as shown in Figures 9(b) and 9(c), respectively, Link 1 of the manipulator initially rotates anticlockwise into the empty region to allow for links 2 and 3 to extend upwards. After the extension of links 2 and 3, link 1 rotates to the final desired position. The resulting motion indicates the ability of the fluid motion planner to create a trajectory in S-space that corresponds to a valid C-space trajectory that avoids collision with the wall obstacles. Figure 10 shows the trajectory in C-space for the scenario, where the locations 0 to 5 corresponds to the poses that result in configurations at time steps $t_0$ to $t_5$, respectively. It can be observed that a natural and continuous trajectory in C-space is achieved utilising the fluid motion planning strategy.

To demonstrate the robustness of the proposed motion planner to different start and end configurations, Figure 11 shows the configurations for an alternative trajectory with a different final configuration. The sequence of 4

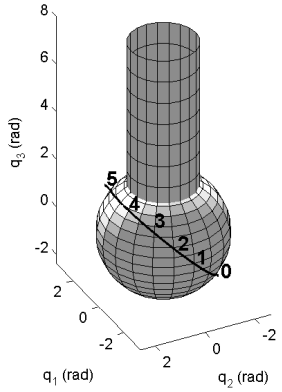


Figure 10: C-space trajectory considering wall obstacle

frames at times $t_0 < t_1 < t_2 < t_3$ show that the resulting trajectory is able to produce a natural motion between the start and end poses while avoiding the wall obstacles as required.

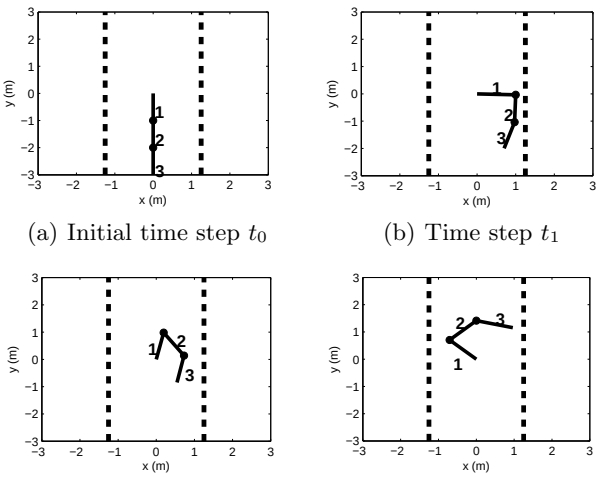


(a) Initial time step $t_0$ (b) Time step $t_1$

(c) Time step $t_2$ (d) Final time step $t_3$

Figure 11: Resulting configurations for trajectory with an alternative final pose

From the results of the different scenarios, it is shown that the proposed motion strategy is able to use the fluid motion planning method in generating collision free trajectories for rigid link manipulators. The proposed algorithm preserves the high computational efficiency of fluid motion planning for mobile robots as the closed form expression for the S-space trajectory velocity $\dot{\mathbf{s}}$ is utilised as a function of time. From $\dot{\mathbf{s}}$, the analytical expressions for the trajectory velocity in C-space can then be derived at each instant of time. This computation needs to be performed for each obstacle avoided, such that the com-

putational cost of the algorithm is proportional to the number of obstacles to be avoided. The development of a varying range of mappings between the C-space and S-space would allow for an increased number of obstacle types to be avoided in the proposed fluid manipulator motion planner. As such, the motion planning strategy can be effective in real-time applications and dynamics environments.

## 6 Conclusion

In this paper, an efficient manipulator motion planning strategy that utilises a fluid motion planning algorithm typically studied in mobile robots is proposed. The fluid motion planner was applied to solve the trajectory generation problem in the C-space of the manipulator. To allow for a larger range of obstacles, a mapping to S-space was proposed, where the trajectory was generated in the S-space. On a 3R manipulator example, the proposed motion planning method was able to generate natural C-space trajectories and manipulator motions from an initial to a desired final configuration, in the presence of obstacles. The synthesis of obstacles shows the potential range of C-space obstacles that can be mapped into the S-space. Future work will focus on synthesis of arbitrary shaped obstacles and the extension to different manipulator topologies, particularly those with higher degrees-of-freedoms.

## References

[Chirikjian and Burdick, 1992] Gregory S. Chirikjian and Joel W. Burdick. A geometric approach to hyper-redundant manipulator obstacle avoidance. *J. Mechan. Design-Trans.*, 114:580–585, 1992.

[Fahimi *et al.*, 2003] Farbod Fahimi, Hashem Ashrafiuon, and C. Nataraj. Obstacle avoidance for spatial hyper-redundant manipulators using harmonic potential functions and the mode shape technique. *J. Robot. Syst.*, 20:23–33, 2003.

[Karaman and Frazzoli, 2011] Sertac Karaman and Emilio Frazzoli. Sampling-based algorithms for optimal motion planning. *Int. J. Robot. Res.*, 30:846–894, 2011.

[Kavraki *et al.*, 1996] Lydia Kavraki, Petr Svestka, Jean-Claude Latombe, and Mark Overmars. Probablistic roadmaps for path planning in high-dimensional configuration spaces. *IEEE T. Robotic Autom.*, 12:566–580, 1996.

[Khatib, 1986] Oussama Khatib. Real-time obstacle avoidance for manipulators and mobile robots. *Int. J. Robot. Res.*, 5:90–98, 1986.

[Kircanski and Timcenko, 1992] Manja Kircanski and Olga Timcenko. A geometric approach to manipulator path planning in 3d space in the presence of obstacles. *Robotica*, 10:321, 1992.

[Kuffner and LaValle, 2000] James Kuffner and Steven LaValle. RRT-connect: An efficient approach to single-quert path planning. In *Proc. IEEE Int. Conf. Rob. Autom.*, pages 995–1001, 2000.

[Li and Bui, 1998] Z.X Li and T.D Bui. Robot path planning using fluid model. *J. Intell. Rob. Syst.*, 21:29–50, 1998.

[Lin *et al.*, 2005] Chien-Chou Lin, Lo-Wei Kuo, and Jen-Hui Chuang. Potential-based path planning for robot manipulators. *J. Robot. Syst.*, 22:313–322, 2005.

[Maciejewski and Fox, 1993] Anthony A. Maciejewski and John J. Fox. Path planning and the topology of configuration space. *IEEE T. Robotic Autom.*, 9:444–456, 1993.

[Mao and Hsia, 1997] Ziqiang Mao and T.C. Hsia. Obstacle avoidance inverse kinematics solution of redundant robots by neural networks. *Robotica*, 15:3–10, 1997.

[Waydo and Murray, 2003] Stephen Waydo and Richard M. Murray. Vehicle motion planning using stream functions. In *Proc. IEEE Int. Conf. Rob. Autom.*, volume 2, pages 2484–2491, 2003.

[Weiss, 1944] P. Weiss. On hydrodynamical images. arbitrary irrotational flow disturbed by a sphere. *Math. Proc. Cambridge Philos. Soc.*, 40:259–261, 1944.

[Yahya and Mohamed, 2009] Samer Yahya and Haider A. F. Mohamed. A geometrical motion planning approach for redundant planar manipulators. *Aust. J. Basic Appl. Sci.*, 3:3757–3770, 2009.

[Yang and Meng, 2000] Simon X. Yang and Max Meng. An efficient neural network method for real-time motion planning with safety consideration. *Robot. Auton. Syst.*, 32:115–128, 2000.

[Zhang *et al.*, 2009] Yunong Zhang, Zhiguo Tan, Ke Chen, Zhi Yang, and Xuanjiao Lv. Repetitive motion of redundant robots planned by three kinds of recurrent neural networks and illustrated with a four-link planar manipulator's straight-line example. *Robot. Auton. Syst.*, 57:645–651, 2009.